Energy-Efficient UAV Communication With Trajectory Optimization

Yong Zeng, *Member, IEEE*, and Rui Zhang, *Fellow, IEEE*

***Abstract*— Wireless communication with unmanned aerial vehicles (UAVs) is a promising technology for future communication systems. In this paper, assuming that the UAV flies horizontally with a fixed altitude, we study energy-efficient UAV communication with a ground terminal via optimizing the UAV's trajectory, a new design paradigm that jointly considers both the communication throughput and the UAV's energy consumption. To this end, we first derive a theoretical model on the propulsion energy consumption of fixed-wing UAVs as a function of the UAV's flying speed, direction, and acceleration. Based on the derived model and by ignoring the radiation and signal processing energy consumption, the energy efficiency of UAV communication is defined as the total information bits communicated normalized by the UAV propulsion energy consumed for a finite time horizon. For the case of unconstrained trajectory optimization, we show that both the rate-maximization and energy-minimization designs lead to vanishing energy efficiency and thus are energy-inefficient in general. Next, we introduce a simple circular UAV trajectory, under which the UAV's flight radius and speed are jointly optimized to maximize the energy efficiency. Furthermore, an efficient design is proposed for maximizing the UAV's energy efficiency with general constraints on the trajectory, including its initial/final locations and velocities, as well as minimum/maximum speed and acceleration. Numerical results show that the proposed designs achieve significantly higher energy efficiency for UAV communication as compared with other benchmark schemes.**

***Index Terms*— UAV communication, energy efficiency, trajectory optimization, sequential convex optimization.**

I. Introduction

WIRELESS communication by leveraging the use of unmanned aerial vehicles (UAVs) has attracted increasing interest recently [1]. Compared to terrestrial communication systems or those based on high-altitude platforms (HAPs), low-altitude UAV systems are in general more cost-effective by enabling on-demand operations, more swift and flexible for deployment and reconfiguration due to the fully controllable UAV mobility, and are likely to have better communication channels due to the higher chance of short-distance line-of-sight (LoS) communication links.

The main applications of UAV-assisted communications can be loosely classified into three categories [1]. The first one is *UAV-aided ubiquitous coverage* [2]–[5], where UAVs are employed to assist the existing terrestrial communication infrastructure, if any, in providing seamless wireless coverage within the serving area. In this case, the UAVs usually stay quasi-stationarily above the serving area acting as aerial base stations (BSs). Two typical scenarios are rapid service recovery after partial or complete infrastructure damage due to natural disasters [6], [7], and BS offloading in hot spots [8], which are two important scenarios to be effectively addressed in the fifth-generation (5G) wireless communication systems [9]. Another promising application is *UAV-aided relaying* [10]–[12], where UAVs are dispatched to provide reliable wireless connectivity between two or more distant users or user groups in adversarial environments, such as between the front line and the command center for emergency responses or military operations. Last but not least, UAV systems could also be employed for *UAV-aided information dissemination/data collection* [13], [14]. This is especially appealing for periodic sensing or Internet of Things (IoT) applications, where UAVs could be dispatched to fly over the sensors for communications to greatly reduce the sensors' operation power and hence prolong the network lifetime.

Despite their ample applications, UAV communication systems face many new challenges [1]. In particular, the endurance and performance of UAV systems are fundamentally limited by the on-board energy, which is practically finite due to the aircraft's size and weight constraints. Thus, energy-efficient communication for maximizing the information bits per unit energy consumption of the UAV is of paramount importance. Note that energy-efficient designs for UAV communication systems are significantly different from those in the existing literature on terrestrial communication systems [15], [16]. Firstly, while the motivation for energy-efficiency maximization in terrestrial communications is mainly for saving energy consumption and cost, that for UAV systems is more critical due to the limited on-board energy. For example, given the maximum amount of energy that can be carried by the aircraft, an improvement in energy efficiency directly increases the amount of information bits that can be communicated with the UAV before it needs to be recalled for recharging/refueling. Secondly, besides the conventional energy expenditure on communication-related functions, such as communication circuits and signal

Manuscript received August 5, 2016; revised November 15, 2016 and February 1, 2017; accepted March 15, 2017. Date of publication March 28, 2017; date of current version June 8, 2017. The associate editor coordinating the review of this paper and approving it for publication was A. Bletsas.

Y. Zeng is with the Department of Electrical and Computer Engineering, National University of Singapore, Singapore 117583 (e-mail: elezeng@nus.edu.sg).

R. Zhang is with the Department of Electrical and Computer Engineering, National University of Singapore, Singapore 117583. He is also with the Institute for Infocomm Research, A*STAR, Singapore 138632 (e-mail: elezhang@nus.edu.sg).

Color versions of one or more of the figures in this paper are available online at http://ieeexplore.ieee.org.

Digital Object Identifier 10.1109/TWC.2017.2688328

transmission, the UAV systems are subject to the additional propulsion power consumption for maintaining the UAV aloft and supporting its mobility (if necessary), which is usually much higher than the communication power consumption. Note that the UAV's propulsion energy consumption is determined by its flying status including velocity and acceleration, which thus needs to be taken into account in energy-efficient design for UAV communications.

In this paper, we study the energy-efficient designs for UAV communication, where a UAV is employed to communicate with a ground terminal (GT) for a finite time horizon. The objective is to maximize the energy efficiency in bits/Joule via optimizing the UAV's trajectory, which is a new design framework that needs to jointly consider the communication throughput and the UAV's propulsion energy consumption. Intuitively, from the throughput maximization perspective, the UAV should stay stationary at the nearest possible location from the GT so as to maintain the best channel condition for communication. However, hovering with strictly zero speed is known to be inefficient (for rotary-wing UAVs) or even impossible (for fixed-wing UAVs) in terms of propulsion energy consumption [17]. Thus, the energy-efficient trajectory design needs to strike an optimal balance between maximizing the communication throughput and minimizing the UAV's propulsion energy consumption. The main contributions of the paper are summarized as follows.

- First, we derive a theoretical model for the propulsion energy consumption of fixed-wing UAVs as a function of the UAV's flying velocity and acceleration, based on which the energy efficiency of UAV communication is defined. Note that fixed-wing UAVs usually have larger payload and higher speed than their rotary-wing counterparts.[1] To the best of our knowledge, the derived model is the first theoretical model that relates the UAV's energy consumption with its velocity (including both flying speed and direction) and acceleration, whereas existing literature mostly uses heuristic energy consumption models only taking into account the speed parameter [18], [19].
- Next, for the case of unconstrained UAV trajectory, we study the energy efficiency of the rate-maximization and energy-minimization designs to gain insights. It is shown that the two designs both lead to vanishing energy efficiency, and hence are energy-inefficient in general.
- We then introduce a practical circular UAV trajectory that is centered at the GT with certain flight radius and speed, which are jointly optimized to maximize the energy efficiency for UAV communication. This result provides a practical design on how a fixed-wing UAV should hover around a GT in order to maximize the communication throughput subject to its limited on-board energy.
- Furthermore, we study the energy-efficiency maximization problem subject to the general constraints on the UAV's trajectory, including those on its initial/final locations and velocities, minimum/maximum speed, and maximum acceleration. An efficient algorithm is proposed to find the approximately optimal trajectory based on linear state-space approximation and sequential convex optimization techniques.

[1]The analysis in this paper can be extended to rotary-wing UAVs with the energy consumption model modified accordingly.

Note that energy-efficient UAV communications have been recently studied [20]–[22], but without considering the UAV's propulsion energy consumption. On the other hand, trajectory optimization for UAV communication systems has been studied for various setups. In [11] and [23], by assuming that the UAV flies with a constant speed, the UAV's heading (or flying direction) is optimized for UAV-assisted wireless relaying and uplink communications, respectively. In [24], a UAV-based mobile relay is used for forwarding independent data to different user groups. The data volume as well as the relay trajectory in terms of the visiting sequence to the different user groups are optimized based on a genetic algorithm. In [25] and [26], the deployment/movement of UAVs is optimized to improve the network connectivity of a UAV-assisted ad-hoc network. In our prior work [12], we study the throughput maximization problem of a UAV-enabled mobile relaying system via joint source/relay power allocation and trajectory optimization. However, none of the above works on trajectory optimization considers the energy efficiency of the system. It is also noted that aircraft trajectory optimization has been studied for other systems not specifically for communication purposes. For instance, mixed-integer linear program (MILP) has been widely applied for trajectory planning for UAV systems to ensure terrain or collision avoidance [27], [28]. The authors in [19] study the energy-aware coverage path planning for aerial imaging purposes with the measurement-based energy model of a specific quadrotor UAV. To the authors' best knowledge, our paper is the first work that studies the energy-efficient UAV communication with a generic UAV energy consumption model, which provides a new framework for designing the UAV trajectory parameters such as its instantaneous velocity and acceleration for communication performance optimization.

The rest of this paper is organized as follows. Section II introduces the system model and defines the energy efficiency for UAV communication based on a theoretically derived model on UAV propulsion energy consumption. In Section III, the energy efficiency of unconstrained trajectory optimization for rate maximization or energy minimization is studied. Section IV considers the circular trajectory for energy efficiency maximization. In Section V, an efficient algorithm is proposed for the generally constrained trajectory optimization for energy efficiency maximization. Section VI presents the numerical results. Finally, we conclude the paper in Section VII.

Notations: In this paper, scalars are denoted by italic letters. Boldface lower-case letters denote vectors. $\mathbb{R}^{M\times 1}$ denotes the space of M-dimensional real-valued vectors. For a vector $\mathbf{a}$, $\|\mathbf{a}\|$ represents its Euclidean norm, and $\mathbf{a}^T$ denotes its transpose. $\ln(\cdot)$ and $\log_2(\cdot)$ denote the natural logarithm and logarithm with base 2, respectively. $\tan^{-1}(\cdot)$ is the inverse tangent function. For a time-dependent function $\mathbf{x}(t)$, $\dot{\mathbf{x}}(t)$ and $\ddot{\mathbf{x}}(t)$

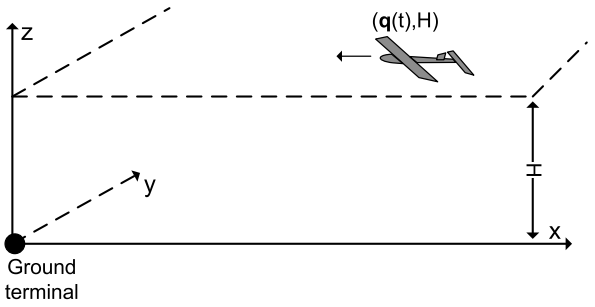

Fig. 1. Point-to-point wireless communication from a UAV to a ground terminal.

denote the first- and second-order derivatives with respect to time t, respectively.

II. System Model and UAV Energy Efficiency

A. System Model

As shown in Fig. 1, we consider a wireless communication system where a UAV is employed to send information to a GT. In practice, wireless communication using only one single UAV is relevant in many scenarios. For example, for delay-tolerant applications such as data collection for periodic sensing, it could be sufficient to deploy only one UAV to communicate with the ground sensors sequentially so as to minimize the cost. As another example, the considered setup could correspond to the emergency service recovery scenario in cellular systems, where the GT corresponds to an isolated BS with the backhaul links destroyed after nature disaster. For the more general scenarios with multiple UAVs and/or multiple GTs, the design for energy efficiency optimization is more intricate, which will be left as future work. Our objective is to optimize the UAV's trajectory so as to maximize the energy efficiency in bits/Joule for a given finite time horizon $T > 0$, where the energy efficiency is defined as the aggregated information bits that are transmitted to the GT normalized by the UAV's total energy consumption over the duration T.

Without loss of generality, we consider a three-dimensional (3D) Cartesian coordinate system such that the GT is located at the origin $(0, 0, 0)$. Furthermore, we assume that the UAV flies horizontally at a constant altitude H. In practice, H could correspond to the minimum altitude required for terrain or building avoidance without the need of frequent aircraft ascending and descending. Denote the UAV trajectory projected on the horizontal plane as $\mathbf{q}(t) = [x(t), y(t)]^T \in \mathbb{R}^{2\times 1}$, where $0 \le t \le T$. Thus, the time-varying distance from the UAV to the GT can be expressed as

$$d(t) = \sqrt{H^2 + \|\mathbf{q}(t)\|^2}, \quad 0 \le t \le T. \tag{1}$$

For ease of exposition, we assume that the communication link from the UAV to the GT is dominated by the LoS channel. Note that in practice, the UAV-ground channel is more likely to have the LoS link as compared to the terrestrial ground-ground channels. The extension to the non-LoS and multi-path fading channels will be left as our future work. Furthermore, the Doppler effect due to the UAV mobility is assumed to be perfectly compensated. Therefore, the time-varying channel follows the free-space path loss model, which can be expressed as

$$h(t) = \beta_0 d^{-2}(t) = \frac{\beta_0}{H^2 + \|\mathbf{q}(t)\|^2}, \ 0 \le t \le T, \tag{2}$$

where β_0 denotes the channel power at the reference distance $d_0 = 1$m. We assume a constant transmission power P by the UAV, which could correspond to the maximum allowable value imposed by the authority regulations. The instantaneous channel capacity in bits/second can be expressed as [29]

$$\begin{aligned} R(t) &= B\log_2\left(1 + \frac{Ph(t)}{\sigma^2}\right) \\ &= B\log_2\left(1 + \frac{\gamma_0}{H^2 + \|\mathbf{q}(t)\|^2}\right), \quad 0 \le t \le T, \end{aligned} \tag{3}$$

where B denotes the channel bandwidth, σ^2 is the white Gaussian noise power at the GT receiver, $\gamma_0 = \beta_0 P/\sigma^2$ is the reference received signal-to-noise ratio (SNR) at $d_0 = 1$m. Note that if the receiver suffers from additional interferences, the aggregate interference is assumed to be of Gaussian distribution and its power can be incorporated into the noise term σ^2. Thus, the total amount of information bits $\bar{R}$ that can be transmitted from the UAV to the GT over the duration T is a function of the UAV trajectory $\mathbf{q}(t)$, expressed as

$$\bar{R}\big(\mathbf{q}(t)\big) = \int_0^T B\log_2\left(1 + \frac{\gamma_0}{H^2 + \|\mathbf{q}(t)\|^2}\right) dt. \tag{4}$$

B. UAV Energy Consumption Model and Energy Efficiency

The total energy consumption of the UAV includes two components. The first one is the communication-related energy, which is due to the radiation, signal processing, as well as other circuitry. The other component is the propulsion energy, which is required for ensuring that the UAV remains aloft as well as for supporting its mobility, if needed. Note that in practice, the communication-related energy is usually much smaller than the UAV's propulsion energy, e.g., a few watts [30] versus hundreds of watts [19], and thus is ignored in this paper. Furthermore, as shown in Appendix A, for fixed-wing UAVs with level flight under normal operations, i.e., no abrupt deceleration that requires the engine to abnormally produce a reverse thrust against the forward motion of the aircraft, the total propulsion energy required is a function of the trajectory $\mathbf{q}(t)$, which is expressed as (5) shown at the bottom of this page, where

$$\mathbf{v}(t) \triangleq \dot{\mathbf{q}}(t), \quad \mathbf{a}(t) \triangleq \ddot{\mathbf{q}}(t) \tag{6}$$

$$\bar{E}(\mathbf{q}(t)) = \int_0^T \left[c_1\|\mathbf{v}(t)\|^3 + \frac{c_2}{\|\mathbf{v}(t)\|}\left(1 + \frac{\|\mathbf{a}(t)\|^2 - \frac{(\mathbf{a}^T(t)\mathbf{v}(t))^2}{\|\mathbf{v}(t)\|^2}}{g^2}\right)\right] dt + \frac{1}{2}m\left(\|\mathbf{v}(T)\|^2 - \|\mathbf{v}(0)\|^2\right). \tag{5}$$

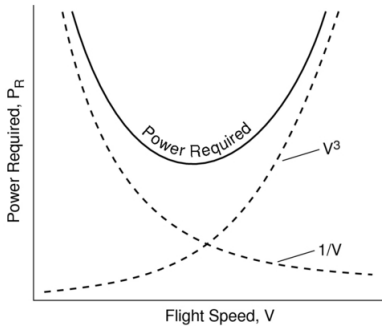

Fig. 2. Typical power required curve versus speed V for a UAV in straight-and-level flight [31].

denote the instantaneous UAV velocity and acceleration vectors, respectively, c_1 and c_2 are two parameters related to the aircraft's weight, wing area, air density, etc., as expressed in (57) of Appendix A, g is the gravitational acceleration with nominal value 9.8 m/s^2, m is the mass of the UAV including all its payload.[2]

The expression in (5) shows that for level flight with fixed altitude, the UAV's energy consumption only depends on the velocity $\mathbf{v}(t)$ and acceleration $\mathbf{a}(t)$, rather than its actual location $\mathbf{q}(t)$. Furthermore, the result in (5) can be interpreted based on the well known work-energy principle. The integral term in (5), which is guaranteed to be positive, is the work required from the aircraft's engine to overcome the air resistance force (or the drag). It depends on the UAV speed $\|\mathbf{v}(t)\|$, as well as its centrifugal acceleration $a_\perp(t) \triangleq \sqrt{\|\mathbf{a}(t)\|^2 - \frac{(\mathbf{a}^T(t)\mathbf{v}(t))^2}{\|\mathbf{v}(t)\|^2}}$, i.e., the acceleration component that is normal to the UAV velocity vector and causing heading (direction) changes without altering the UAV speed. The second term in (5), denoted as Δ_K, represents the change in the UAV's kinetic energy, an aggregated effect of the UAV's tangential acceleration component that is in parallel to the UAV's velocity vector. Thus, Δ_K only depends on the initial and final speeds $\|\mathbf{v}(T)\|$ and $\|\mathbf{v}(0)\|$, rather than the intermediate UAV state. Note that if $\|\mathbf{v}(t')\| = 0$ for some t', then the required energy $\bar{E} \to \infty$, which reflects the fact that a fixed-wing aircraft must maintain a forward motion to remain aloft.

To have a sanity check on the derived energy consumption model, we first consider the special case of steady straight-and-level flight (SLF) with constant speed V, i.e., $\|\mathbf{v}(t)\| = V$ and $\mathbf{a}(t) = \mathbf{0}$, $\forall t$. In this case, (5) reduces to

$$\bar{E}_{\rm SLF}(V) = T\left(c_1 V^3 + \frac{c_2}{V}\right). \tag{7}$$

This corresponds to the classic aircraft power consumption model known in aerodynamics theory [31]. The power consumption of (7) as a function of V is illustrated in Fig. 2, which consists of two terms. The first term, which is proportional to the cube of the speed V, is known as the *parasitic power* for overcoming the parasitic drag due to the aircraft's skin friction, form drag, etc. The second term, which is inversely proportional to V, is known as the *induced power* for overcoming the lift-induced drag, i.e., the resulting drag force due to wings redirecting air to generate the lift for compensating the aircraft's weight [17].

Next, we consider another special trajectory where the UAV flies at a constant speed V but with possibly time-varying headings. In this case, we have $\|\mathbf{v}(t)\| = V$ and $\mathbf{a}^T(t)\mathbf{v}(t) = 0$, $\forall t$. Thus, (5) reduces to

$$\bar{E}(V, a(t)) = \bar{E}_{\rm SLF}(V) + \frac{c_2}{Vg^2}\int_0^T a^2(t)dt, \tag{8}$$

where $\bar{E}_{\rm SLF}(V)$ is given in (7), and $a(t) \triangleq \|\mathbf{a}(t)\|$ is the magnitude of the acceleration vector $\mathbf{a}(t)$, which is always perpendicular to the UAV flying direction for maintaining the constant speed. The expression in (8) clearly shows that for the same flying speed, direction changing consumes additional energy as compared to straight flight, as expected. For the general UAV trajectory where the energy consumption model (5) cannot be further simplified, practical experiments could be conducted to validate the derived theoretical model.

With (4) and (5), the energy efficiency of the UAV communication system can thus be expressed as

$$\mathrm{EE}(\mathbf{q}(t)) = \frac{\bar{R}(\mathbf{q}(t))}{\bar{E}(\mathbf{q}(t))}. \tag{9}$$

III. Energy Efficiency With Unconstrained Trajectory

This section aims to give a simple illustration on the new trade-off between rate maximization and energy minimization via trajectory design for UAV communications. For ease of exposition and to gain essential insights, we consider the ideal case of unconstrained UAV trajectory design, whereas the generally constrained trajectory optimization will be studied in Section V.

First, we study the rate-maximization trajectory without considering the UAV energy consumption. In the absence of any constraint on $\mathbf{q}(t)$, it immediately follows from (4) that the rate-maximization (rm) UAV trajectory should be $\mathbf{q}(t) = \mathbf{0}$, $\forall t$, i.e., the UAV should stay stationary just above the GT to maintain the best communication channel. The resulting aggregated information throughput is $\bar{R}_{\rm rm} = TB\log_2\left(1 + \frac{\gamma_0}{H^2}\right)$. In this case, since $\mathbf{v}(t) = \dot{\mathbf{q}}(t) = \mathbf{0}$, $\forall t$, the corresponding energy consumption in (5) is $\bar{E}_{\rm rm} \to \infty$. Thus, the resulting energy efficiency with the rate-maximization trajectory is $\mathrm{EE}_{\rm rm} = \bar{R}_{\rm rm}/\bar{E}_{\rm rm} = 0$, $\forall T > 0$, which is evidently energy-inefficient.

Next, we consider the energy-minimization design, i.e., the UAV trajectory $\mathbf{q}(t)$ is optimized merely for minimizing the total energy consumption without considering the communication performance. By ignoring the change in kinetic energy in the last term of (5), which is independent of the time duration T and hence is practically negligible for large T, the energy-minimization trajectory design problem can be formulated as

$$\min_{\mathbf{v}(t),\mathbf{a}(t)} \int_0^T \left[c_1\|\mathbf{v}(t)\|^3 + \frac{c_2}{\|\mathbf{v}(t)\|}\left(1 + \frac{\|\mathbf{a}(t)\|^2 - \frac{(\mathbf{a}^T(t)\mathbf{v}(t))^2}{\|\mathbf{v}(t)\|^2}}{g^2}\right)\right]dt$$
$$\text{s.t. } \mathbf{a}(t) = \dot{\mathbf{v}}(t), \quad \forall\ 0 \le t \le T. \tag{10}$$

[2]For simplicity, we ignore the aircraft's weight change as more fuel or battery is consumed over time.

Theorem 1: The optimal solution to the energy-minimization (em) problem (10) *is*

$$\mathbf{a}^\star(t) = \mathbf{0},\ \mathbf{v}^\star(t) = V_{\rm em}\vec{\mathbf{v}},\ \forall t, \tag{11}$$

where $V_{\rm em} \triangleq (c_2/(3c_1))^{1/4}$ *is the energy-minimum speed and* $\vec{\mathbf{v}}$ *is an arbitrary unit-norm vector denoting the constant UAV flying direction. The corresponding minimum energy consumption is*

$$\bar{E}_{\rm em} = P_{\min} T, \tag{12}$$

with $P_{\min} \triangleq \left(3^{-3/4} + 3^{1/4}\right) c_1^{1/4} c_2^{3/4}$ *denoting the minimum power consumption of the UAV.*

Proof: Please refer to Appendix B. ∎

Theorem 1 shows that for the unconstrained trajectory optimization, the energy-minimization solution is simply the steady straight-and-level flight with the power-minimum speed $V_{\rm em}$. Note that the energy-minimization trajectory is non-unique, since the initial UAV location $\mathbf{q}(0)$ and the flying direction $\vec{\mathbf{v}}$ can be arbitrary. It is not difficult to show that among all the energy-minimization trajectories, i.e., all straight-and-level flights with the energy-minimum speed $V_{\rm em}$, those being symmetric around the GT (or the origin) lead to the highest information throughput. Therefore, without loss of optimality, the trajectory can be expressed as $\mathbf{q}(t) = [x(t), 0]^T$, where $x(t) = -V_{\rm em}T/2 + V_{\rm em}t,\ 0 \le t \le T$. By substituting $\mathbf{q}(t)$ into (4), the maximum aggregated information throughput by the energy-minimization trajectory design can be expressed as

$$\begin{aligned}
&\bar{R}_{\rm em} \\
&= B\int_0^T \log_2\left(1 + \frac{\gamma_0}{H^2 + (-\frac{V_{\rm em}T}{2} + V_{\rm em}t)^2}\right)dt \\
&= \frac{4B}{(\ln 2)V_{\rm em}}\left[\frac{V_{\rm em}T}{4}\ln\left(1 + \frac{\gamma_0}{H^2 + (\frac{V_{\rm em}T}{2})^2}\right)\right. \\
&\quad \left. + \sqrt{H^2+\gamma_0}\tan^{-1}\left(\frac{V_{\rm em}T}{2\sqrt{H^2+\gamma_0}}\right) - H\tan^{-1}\left(\frac{V_{\rm em}T}{2H}\right)\right],
\end{aligned} \tag{13}$$

where (13) follows from the change of variable $z = -\frac{V_{\rm em}T}{2} + V_{\rm em}t$ and the integral formula given in (14) shown on the bottom of this page.

As a result, the maximum energy efficiency achievable by the energy-minimization trajectory design can be obtained in closed-form as $\mathrm{EE}_{\rm em} = \bar{R}_{\rm em}/\bar{E}_{\rm em}$. For sufficiently large operation duration $T \to \infty$, the aggregated information throughput in (13) reduces to

$$R_{\rm em} \to \frac{2\pi B}{(\ln 2)V_{\rm em}}\left(\sqrt{H^2+\gamma_0} - H\right),\ \text{as } T \to \infty, \tag{15}$$

which is finite and independent of T. On the other hand, as the minimum energy consumption in (12) linearly increases with T, the resulting energy efficiency is thus $\mathrm{EE}_{\rm em} \to 0$, as $T \to \infty$. Thus, the energy-minimization trajectory design is also energy-inefficient in general.

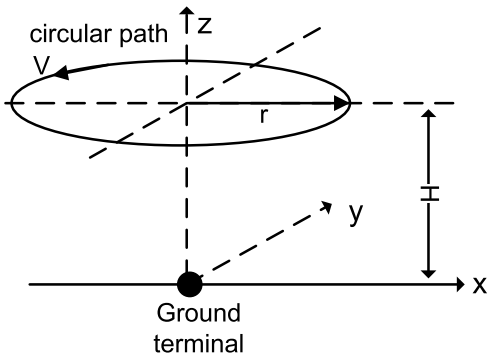

Fig. 3. An illustration of the steady circular flight.

IV. Energy-Efficiency Maximization With Circular Trajectory

The preceding section shows that neither the rate-maximization nor the energy-minimization trajectory design is energy-efficient. In general, energy-efficient trajectory design needs to achieve an optimal tradeoff between these two objectives. To obtain a mathematically tractable analysis on such a tradeoff, in this section, we propose an energy-efficient design by assuming that the UAV follows a simple circular trajectory centered at the GT, for which the UAV energy efficiency defined in (9) reduces to a much simpler closed-form expression (see (18)). Note that with circular trajectory, the UAV could hover around the GT with smooth turning angles, for which a balance between rate maximization and energy minimization can be flexibly controlled via adjusting the trajectory radius. Specifically, let V denote the constant speed of the UAV and r denote the radius of the circular trajectory, as illustrated in Fig. 3. Intuitively, a smaller radius r, though achieving higher information throughput with the GT, also consumes more power by the UAV to maintain a more acute heading change, and vice versa. Therefore, both V and r need to be optimized for maximizing the energy efficiency.

With circular (cir) trajectory, it follows from (4) that the aggregated information throughput reduces to a function of the radius r as

$$\bar{R}_{\rm cir}(r) = TB\log_2\left(1 + \frac{\gamma_0}{H^2 + r^2}\right). \tag{16}$$

Note that $\bar{R}_{\rm cir}(r)$ is maximized when $r = 0$, i.e., the rate-maximization circular flight reduces to the extreme case of stationary hovering as studied in Section III, which is known to be energy-inefficient.

On the other hand, for steady circular flight with constant speed V, we have $\|\mathbf{v}(t)\| = V$ and $\mathbf{a}^T(t)\mathbf{v}(t) = 0,\ \forall t$, i.e., the acceleration (if any) must be perpendicular to the velocity to

$$F(z) \triangleq \int \ln\left(1 + \frac{\gamma_0}{H^2+z^2}\right)dz = z\ln\left(1 + \frac{\gamma_0}{H^2+z^2}\right) + 2\sqrt{H^2+\gamma_0}\tan^{-1}\left(\frac{z}{\sqrt{H^2+\gamma_0}}\right) - 2H\tan^{-1}\left(\frac{z}{H}\right). \tag{14}$$

ensure no speed variation. Furthermore, the magnitude of the acceleration for maintaining the circular path is time-invariant and given by $a(t) = \|\mathbf{a}(t)\| = V^2/r, \forall t$ [32]. It then follows from (8) that the UAV energy consumption with steady circular flight further reduces to

$$\bar{E}_{\text{cir}}(V, r) = T\left[\left(c_1 + \frac{c_2}{g^2 r^2}\right)V^3 + \frac{c_2}{V}\right]. \tag{17}$$

It is not difficult to find that $\bar{E}_{\text{cir}}(V, r)$ is minimized when $r \to \infty$ and $V = V_{\text{em}}$, i.e., the energy-minimization circular flight reduces to the extreme case of straight flight with energy-minimum speed V_{em}, which has also been shown to be energy-inefficient in Section III.

With (16) and (17), the energy efficiency in (9) for circular trajectory reduces to

$$\text{EE}_{\text{cir}}(V, r) = \frac{\bar{R}_{\text{cir}}(r)}{\bar{E}_{\text{cir}}(V, r)} = \frac{B\log_2\left(1 + \frac{\gamma_0}{H^2 + r^2}\right)}{\left(c_1 + \frac{c_2}{g^2 r^2}\right)V^3 + \frac{c_2}{V}}. \tag{18}$$

Note that the energy efficiency in (18) is independent of T. The energy-efficiency maximization problem can then be formulated as

$$\max_{V \geq 0, r \geq 0} \text{EE}_{\text{cir}}(V, r). \tag{19}$$

To solve problem (19), it is first noted that the numerator of $\text{EE}_{\text{cir}}(V, r)$ in (18) is independent of the UAV speed V. Thus, for any fixed radius r, the optimal speed V is obtained by minimizing the denominator of (18), which can be readily obtained as

$$V^{\star}_{\text{cir}}(r) = \left(\frac{c_2}{3(c_1 + c_2/(g^2 r^2))}\right)^{1/4}. \tag{20}$$

The corresponding UAV power consumption, i.e., the denominator of (18), reduces to a univariate function of r as

$$P^{\star}_{\text{cir}}(r) = \left(3^{-3/4} + 3^{1/4}\right) c_2^{3/4}\left(c_1 + \frac{c_2}{g^2 r^2}\right)^{1/4}. \tag{21}$$

Thus, by discarding the constant terms and defining $z = r^2$, problem (19) reduces to a univariate optimization problem given by

$$\max_{z \geq 0} \eta(z) \triangleq \frac{\ln\left(1 + \frac{\gamma_0}{H^2 + z}\right)}{\left(c_1 + \frac{c_2}{g^2 z}\right)^{1/4}}. \tag{22}$$

Since $\eta(0) = 0$ and $\lim_{z \to \infty} \eta(z) \to 0$, there must exist a finite optimal solution $z^{\star}$ to problem (22), which can be efficiently found numerically. Furthermore, in the low-SNR regime with $\gamma_0 \ll H^2$, by applying the result $\ln(1 + x) \approx x$ if $x \ll 1$, the optimal solution to (22) can be obtained in closed-form as

$$z^{\star} = \frac{3c_2}{8c_1 g^2}\left[\left(1 + \frac{16H^2 c_1 g^2}{9c_2}\right)^{1/2} - 1\right]. \tag{23}$$

As the optimal value to problem (22) is guaranteed to be positive, a strictly positive energy efficiency is always achievable by the optimized circular trajectory for any $T > 0$, which demonstrates its superiority over the rate-maximization or energy-minimization designs considered in Section III.

V. Energy Efficiency Maximization With Generally Constrained Trajectory

The preceding two sections study the energy efficiency for unconstrained trajectory designs. In practice, the UAV's trajectory $\mathbf{q}(t)$ may need to satisfy a number of practical constraints, such as those on its initial/final states (including location and velocity) and the minimum/maximum speed and maximum acceleration. They are mathematically expressed as

$$C_1: \ \mathbf{q}(0) = \mathbf{q}_0 \tag{24}$$

$$C_2: \ \mathbf{q}(T) = \mathbf{q}_F \tag{25}$$

$$C_3: \ V_{\min} \leq \|\mathbf{v}(t)\| \leq V_{\max}, \forall t \tag{26}$$

$$C_4: \ \mathbf{v}(0) = \mathbf{v}_0 \tag{27}$$

$$C_5: \ \mathbf{v}(T) = \mathbf{v}_F \tag{28}$$

$$C_6: \ \|\mathbf{a}(t)\| \leq a_{\max}, \forall t, \tag{29}$$

where $\mathbf{q}_0, \mathbf{q}_F \in \mathbb{R}^{2\times 1}$ denote the UAV's destined initial and final locations, respectively, $\mathbf{v}_0, \mathbf{v}_F \in \mathbb{R}^{2\times 1}$ are the desired initial and final velocities, respectively, $V_{\max}$ and $a_{\max}$ represent the maximum speed and acceleration, respectively, and $V_{\min}$ represents the minimum speed (or the stall speed) for the fixed-wing UAV to remain aloft.[3] Note that for an aircraft in banked level turn, the acceleration constraint C_6 implicitly imposes a constraint on the bank angle ϕ (correspondingly the turning angle). This can be seen by using (62) in Appendix A, which yields $g\tan\phi = |a_{\perp}(t)| \leq \|\mathbf{a}(t)\| \leq a_{\max}$, with $a_{\perp}(t)$ denoting the centrifugal acceleration component of $\mathbf{a}(t)$. Besides the above constraints, the UAV trajectory design may be subject to other practical constraints due to e.g., terrain avoidance and space restrictions, which will be considered in our future work.

The energy-efficiency maximization problem for constrained trajectories can be formulated as

$$\begin{aligned}(\text{P1}): \quad &\max_{\mathbf{q}(t)} \ \text{EE}(\mathbf{q}(t)) \\ &\text{s.t. } C_1\text{–}C_6,\end{aligned}$$

where $\text{EE}(\mathbf{q}(t))$ is given in (9). Problem (P1) is difficult to be directly solved for two reasons. Firstly, it requires the optimization of the continuous function $\mathbf{q}(t)$, as well as its first- and second-order derivatives $\mathbf{v}(t)$ and $\mathbf{a}(t)$, which essentially involves an infinite number of optimization variables. Secondly, the objective function in $\text{EE}(\mathbf{q}(t))$ is given by the fraction of two integrals, which both lack closed-form expressions. In the following, an efficient algorithm is proposed for (P1) based on two main techniques: discrete linear state-space approximation and sequential convex optimization.

To this end, it is first noted that the energy consumption in (5) can be upper-bounded by

$$\begin{aligned}\bar{E}(\mathbf{q}(t)) \leq &\int_0^T \left[c_1\|\mathbf{v}(t)\|^3 + \frac{c_2}{\|\mathbf{v}(t)\|}\left(1 + \frac{\|\mathbf{a}(t)\|^2}{g^2}\right)\right]dt \\ &+ \Delta_K \triangleq \bar{E}_{\text{ub}}(\mathbf{q}(t)),\end{aligned} \tag{30}$$

with $\Delta_K \triangleq \frac{1}{2}m\left(\|\mathbf{v}(T)\|^2 - \|\mathbf{v}(0)\|^2\right)$ denoting the change of the UAV's kinetic energy, which is fixed with the initial

[3]Note that in practice, the stall speed increases when the aircraft is in maneuvering status (such as turning), but this aspect is not exploited here for simplicity.

and final velocity constraints C_4 and C_5. Note that the upper bound in (30) is tight for constant-speed flight, in which case $\mathbf{a}(t)^T\mathbf{v}(t) = 0$, $\forall t$. Therefore, the energy efficiency in (9) is lower-bounded by

$$\begin{aligned}\mathrm{EE}(\mathbf{q}(t)) &\geq \mathrm{EE}_{\mathrm{lb}}(\mathbf{q}(t)) \triangleq \frac{\bar{R}(\mathbf{q}(t))}{\bar{E}_{\mathrm{ub}}(\mathbf{q}(t))} \\ &= \frac{B\int_0^T \log_2\left(1+\frac{\gamma_0}{H^2+\|\mathbf{q}(t)\|^2}\right)dt}{\int_0^T\left[c_1\|\mathbf{v}(t)\|^3+\frac{c_2}{\|\mathbf{v}(t)\|}\left(1+\frac{\|\mathbf{a}(t)\|^2}{g^2}\right)\right]dt+\Delta_K}.\end{aligned} \tag{31}$$

Thus, (P1) can be approximately solved by maximizing its lower bound as

$$(\mathrm{P1}'): \quad \max_{\mathbf{q}(t)} \ \mathrm{EE}_{\mathrm{lb}}(\mathbf{q}(t)) \quad \text{s.t. } C_1\text{–}C_6. \tag{32}$$

To obtain a more tractable optimization problem, we apply the discrete linear state-space approximation to (P1′). Since $\mathbf{v}(t) \triangleq \dot{\mathbf{q}}(t)$ and $\mathbf{a}(t) \triangleq \dot{\mathbf{v}}(t)$ are respectively the time-varying velocity and acceleration vectors associated with the UAV trajectory $\mathbf{q}(t)$, for any infinitesimal time step δ_t, we have the following results based on the first- and second-order Taylor approximations,

$$\mathbf{v}(t+\delta_t) \approx \mathbf{v}(t) + \mathbf{a}(t)\delta_t, \ \forall t, \tag{33}$$

$$\mathbf{q}(t+\delta_t) \approx \mathbf{q}(t) + \mathbf{v}(t)\delta_t + \frac{1}{2}\mathbf{a}(t)\delta_t^2, \quad \forall t. \tag{34}$$

As a result, by discretizing the time horizon T into $N+2$ slots with step size δ_t, i.e., $t = n\delta_t$, $n = 0, 1, \cdots, N+1$, the UAV's trajectory $\mathbf{q}(t)$ can be well characterized by the discrete-time UAV location $\mathbf{q}[n] \triangleq \mathbf{q}(n\delta_t)$, the velocity $\mathbf{v}[n] \triangleq \mathbf{v}(n\delta_t)$, as well as the acceleration $\mathbf{a}[n] \triangleq \mathbf{a}(n\delta_t)$, $n = 0, 1, \cdots, N+1$. As a result, we have the following discrete state-space model based on (33) and (34),

$$\mathbf{v}[n+1] = \mathbf{v}[n] + \mathbf{a}[n]\delta_t, \tag{35}$$

$$\mathbf{q}[n+1] = \mathbf{q}[n] + \mathbf{v}[n]\delta_t + \frac{1}{2}\mathbf{a}[n]\delta_t^2, \quad n = 0, 1, \cdots N, \tag{36}$$

which is linear with respect to $\mathbf{q}[n]$, $\mathbf{v}[n]$ and $\mathbf{a}[n]$. As a result, problem (P1′) can be rewritten as

(P2):

$$\max_{\substack{\{\mathbf{q}[n],\mathbf{v}[n]\\ \mathbf{a}[n]\}}} \frac{B\sum_{n=1}^N \log_2\left(1+\frac{\gamma_0}{H^2+\|\mathbf{q}[n]\|^2}\right)}{\sum_{n=1}^N\left(c_1\|\mathbf{v}[n]\|^3+\frac{c_2}{\|\mathbf{v}[n]\|}\left(1+\frac{\|\mathbf{a}[n]\|^2}{g^2}\right)\right)+\frac{\Delta_K}{\delta_t}}$$

$$\text{s.t. } \mathbf{q}[n+1] = \mathbf{q}[n] + \mathbf{v}[n]\delta_t + \frac{1}{2}\mathbf{a}[n]\delta_t^2, \quad n = 0, \cdots, N \tag{37}$$

$$\mathbf{v}[n+1] = \mathbf{v}[n] + \mathbf{a}[n]\delta_t, \quad n = 0, \cdots, N \tag{38}$$

$$\mathbf{q}[0] = \mathbf{q}_0, \ \mathbf{q}[N+1] = \mathbf{q}_F \tag{39}$$

$$\mathbf{v}[0] = \mathbf{v}_0, \quad \mathbf{v}[N+1] = \mathbf{v}_F \tag{40}$$

$$\|\mathbf{v}[n]\| \leq V_{\max}, \quad n = 1, \cdots, N \tag{41}$$

$$\|\mathbf{a}[n]\| \leq a_{\max}, \quad n = 0, \cdots, N \tag{42}$$

$$\|\mathbf{v}[n]\| \geq V_{\min}, \quad n = 1, \cdots, N, \tag{43}$$

where (39)–(43) represent the discrete equivalents of C_1–C_6.

Note that the constraints (37)–(42) of problem (P2) are all convex. However, the minimum speed constraint (43) is non-convex, and the objective is a fractional function with a non-concave numerator over a non-convex denominator, and hence (P2) is neither a convex nor quasi-convex problem, which thus cannot be directly solved with the standard convex optimization techniques. Fortunately, by applying the sequential convex optimization technique, an efficient solution can be obtained which is guaranteed to satisfy the Karush-Kuhn-Tucker (KKT) conditions of (P2). This implies that at least a local optimal solution can be found for the problem. To this end, we first reformulate (P2) by introducing slack variables $\{\tau_n\}$ as

(P2.1):

$$\max_{\substack{\{\mathbf{q}[n],\mathbf{v}[n]\\ \mathbf{a}[n],\tau_n\}}} \frac{B\sum_{n=1}^N \log_2\left(1+\frac{\gamma_0}{H^2+\|\mathbf{q}[n]\|^2}\right)}{\sum_{n=1}^N\left(c_1\|\mathbf{v}[n]\|^3+\frac{c_2}{\tau_n}+\frac{c_2\|\mathbf{a}[n]\|^2}{g^2\tau_n}\right)+\frac{\Delta_K}{\delta_t}}$$

$$\text{s.t. (37)–(42)},$$

$$\tau_n \geq V_{\min}, \quad \forall n, \tag{44}$$

$$\|\mathbf{v}[n]\|^2 \geq \tau_n^2, \quad \forall n. \tag{45}$$

It can be shown that at the optimal solution to (P2.1), we must have $\tau_n = \|\mathbf{v}[n]\|$, $\forall n$, since otherwise one can always increase τ_n to obtain a strictly larger objective value. Thus, (P2.1) is equivalent to (P2). With such a reformulation, the denominator of the objective function in (P2.1) is now jointly convex with respect to $\{\mathbf{v}[n], \mathbf{a}[n], \tau_n\}$, but with the new non-convex constraint (45). To tackle this non-convex constraint, a local convex approximation is applied. Specifically, since $\|\mathbf{v}[n]\|^2$ is a convex and differentiable function with respect to $\mathbf{v}[n]$, for any local point $\{\mathbf{v}_j[n]\}$ obtained at the jth iteration, we have

$$\begin{aligned}\|\mathbf{v}[n]\|^2 &\geq \|\mathbf{v}_j[n]\|^2 + 2\mathbf{v}_j^T[n]\left(\mathbf{v}[n]-\mathbf{v}_j[n]\right) \\ &\triangleq \psi_{\mathrm{lb}}(\mathbf{v}[n]), \quad \forall \mathbf{v}[n],\end{aligned} \tag{46}$$

where the equality holds at the point $\mathbf{v}[n] = \mathbf{v}_j[n]$. Note that (46) follows from the fact that the first-order Taylor expansion of a convex differentiable function is its global under-estimator [33]. Furthermore, at the local point $\mathbf{v}_j[n]$, both the function $\|\mathbf{v}[n]\|^2$ and its lower bound $\psi_{\mathrm{lb}}(\mathbf{v}[n])$ have the identical gradient, which is equal to $2\mathbf{v}_j[n]$.

Define the new constraint,

$$\psi_{\mathrm{lb}}(\mathbf{v}[n]) \geq \tau_n^2, \quad \forall n, \tag{47}$$

which is convex since $\psi_{\mathrm{lb}}(\mathbf{v}[n])$ is linear with respect to $\mathbf{v}[n]$. Then the inequality in (46) shows that the convex constraint (47) always implies the non-convex constraint (45), but the reverse is not true in general.

Similarly, to tackle the non-concavity of the numerator of the objective function in (P2.1), for any local point $\{\mathbf{q}_j[n]\}$ obtained at the jth iteration, define the function

$$\bar{R}_{\mathrm{lb}}(\{\mathbf{q}[n]\}) = B\sum_{n=1}^N\left[\alpha_j[n]-\beta_j[n]\left(\|\mathbf{q}[n]\|^2-\|\mathbf{q}_j[n]\|^2\right)\right], \tag{48}$$

where

$$\alpha_j[n] = \log_2\left(1+\frac{\gamma_0}{H^2+\|\mathbf{q}_j[n]\|^2}\right), \tag{49}$$

$$\beta_j[n] = \frac{(\log_2 e)\gamma_0}{(H^2+\gamma_0+\|\mathbf{q}_j[n]\|^2)(H^2+\|\mathbf{q}_j[n]\|^2)}, \quad \forall n. \tag{50}$$

Note that $\bar{R}_{\rm lb}(\{\mathbf{q}[n]\})$ is a concave function with respect to $\{\mathbf{q}[n]\}$. Furthermore, we have the following result.

Theorem 2: For any given $\{\mathbf{q}_j[n]\}$, we have

$$\bar{R}(\{\mathbf{q}[n]\}) \triangleq B\sum_{n=1}^{N}\log_2\left(1+\frac{\gamma_0}{H^2+\|\mathbf{q}[n]\|^2}\right) \geq \bar{R}_{\rm lb}(\{\mathbf{q}[n]\}), \quad \forall \mathbf{q}[n], \tag{51}$$

where the equality holds at the point $\mathbf{q}[n]=\mathbf{q}_j[n]$, $\forall n$. Furthermore, at the point $\mathbf{q}[n]=\mathbf{q}_j[n]$, $\forall n$, both $\bar{R}(\{\mathbf{q}[n]\})$ and $\bar{R}_{\rm lb}(\{\mathbf{q}[n]\})$ have identical gradient, i.e., $\nabla\bar{R}=\nabla\bar{R}_{\rm lb}$.

Proof: The proof of the lower bound in (51) follows similar arguments as that for [12, Lemma 2]. We first define the function $h(z)\triangleq\log_2\left(1+\frac{\gamma}{A+z}\right)$ for some constant $\gamma\geq 0$ and A, which can be shown to be convex for $A+z\geq 0$. Using the property that the first-order Taylor expansion of a convex function is a global under-estimator [33], for any given z_0, we have $h(z)\geq h(z_0)+h'(z_0)(z-z_0)$, $\forall z$, where $h'(z_0)=\frac{-(\log_2 e)\gamma}{(A+z_0)(A+\gamma+z_0)}$ is the derivative of $h(z)$ at point z_0. By letting $z_0=0$, we have the following inequality,

$$\log_2\left(1+\frac{\gamma}{A+z}\right)\geq\log_2\left(1+\frac{\gamma}{A}\right)-\frac{(\log_2 e)\gamma z}{A(A+\gamma)}, \quad \forall z. \tag{52}$$

Then for each time slot n, let $\gamma=\gamma_0$, $A=H^2+\|\mathbf{q}_j[n]\|^2$, $z=\|\mathbf{q}[n]\|^2-\|\mathbf{q}_j[n]\|^2$, the inequality in (51) thus follows.

Furthermore, it can be obtained from (48) that for any n, the gradient of $\bar{R}_{\rm lb}$ with respect to $\mathbf{q}[n]$ is

$$\nabla_{\mathbf{q}[n]}\bar{R}_{\rm lb}=-2B\beta_j[n]\mathbf{q}[n], \quad \forall n. \tag{53}$$

The gradient of $\bar{R}$ in (51) can be obtained as

$$\nabla_{\mathbf{q}[n]}\bar{R}=\frac{-2B(\log_2 e)\gamma_0\mathbf{q}[n]}{(H^2+\gamma_0+\|\mathbf{q}[n]\|^2)(H^2+\|\mathbf{q}[n]\|^2)}, \quad \forall n. \tag{54}$$

The two gradients in (53) and (54) are identical when evaluated at $\mathbf{q}[n]=\mathbf{q}_j[n]$, $\forall n$. ■

As a result, for any given local point $\{\mathbf{q}_j[n],\mathbf{v}_j[n]\}$, define the following optimization problem,

$$\text{(P2.2)}: \max_{\substack{\{\mathbf{q}[n],\mathbf{v}[n]\\ \mathbf{a}[n],\tau_n\}}} \frac{\bar{R}_{\rm lb}(\{\mathbf{q}[n]\})}{\sum_{n=1}^{N}\left(c_1\|\mathbf{v}[n]\|^3+\frac{c_2}{\tau_n}+\frac{c_2\|\mathbf{a}[n]\|^2}{g^2\tau_n}\right)+\frac{\Delta_K}{\delta_t}}$$
$$\text{s.t. (37)–(42)},$$
$$\tau_n\geq V_{\min}, \quad \forall n,$$
$$\psi_{\rm lb}(\mathbf{v}[n])\geq\tau_n^2, \forall n.$$

Based on the previous discussions, it readily follows that the objective value of (P2.2) gives a lower bound to that of problem (P2.1). Furthermore, problem (P2.2) is a fractional maximization problem, with a concave numerator and a convex denominator, as well as all convex constraints. Thus, (P2.2) can be efficiently solved via the bisection method [33] or the standard Dinkelbach's algorithm for fractional programming [34].

Thus, the original non-convex problem (P2.1) can be solved by iteratively optimizing (P2.2) with the local point $\{\mathbf{q}_j[n],\mathbf{v}_j[n]\}$ updated in each iteration, which is summarized in Algorithm 1.

Algorithm 1 Sequential Convex Optimization for (P2.1)

1: Initialize $\mathbf{q}_0[n]$, $\mathbf{v}_0[n]$, $\forall n$. Let $j=0$.
2: **repeat**
3: Solve problem (P2.2) for the given local point $\{\mathbf{q}_j[n],\mathbf{v}_j[n]\}$, and denote the optimal solution as $\{\mathbf{q}_j^*[n],\mathbf{v}_j^*[n]\}$.
4: Update the local point $\mathbf{q}_{j+1}[n]=\mathbf{q}_j^*[n]$ and $\mathbf{v}_{j+1}[n]=\mathbf{v}_j^*[n]$, $\forall n$.
5: Update $j=j+1$.
6: **until** The fractional increase of the objective value of (P2.1) is below a threshold ϵ.

Let $\text{EE}_{\text{lb},j}^*$ denote the corresponding optimal value of (P2.1) obtained via Algorithm 1 at the jth iteration. We have the following result.

Lemma 1: The energy efficiency lower bound $\text{EE}_{\text{lb},j}^*$ obtained in Algorithm 1 is monotonically non-decreasing, i.e., $\text{EE}_{\text{lb},j}^*\geq\text{EE}_{\text{lb},j-1}^*$, $\forall j\geq 1$. Furthermore, the sequence $\{\mathbf{q}_j^*[n],\mathbf{v}_j^*[n]\}$, $j=0,1,\cdots$, converges to a point fulfilling the KKT optimality conditions of the original non-convex problem (P2.1).

Proof: Lemma 1 directly follows from [35, Proposition 3], by making use of Theorem 2 as well as the fact that the lower bound $\psi_{\rm lb}(\mathbf{v}[n])$ has both identical value and identical gradient as $\|\mathbf{v}[n]\|^2$ at the local point $\mathbf{v}[n]=\mathbf{v}_j[n]$. The details are omitted for brevity. ■

Note that since each iteration of Algorithm 1 requires solving convex optimization problems, the proposed algorithm has a polynomial complexity in the worst case [33]. Furthermore, the trajectory optimization problem can be solved off-line before the UAV dispatch at the ground control station with a high computational capability. As a final remark, it is noted that Algorithm 1 can also be applied for energy efficiency maximization with unconstrained trajectory optimization by discarding C_1–C_6, which gives an alternative energy-efficient design without restricting to circular trajectory considered in Section IV. Furthermore, Algorithm 1 can be similarly applied for the rate-maximization and energy-minimization designs for constrained trajectories with the constraints C_1–C_6, since they correspond to the special cases of (P2) by only maximizing/minimizing the numerator and denominator, respectively. These special cases will be considered in the numerical simulations given in the next section.

VI. Numerical Results

In this section, numerical results are provided to validate the proposed design. The UAV altitude is fixed at $H=100$m.

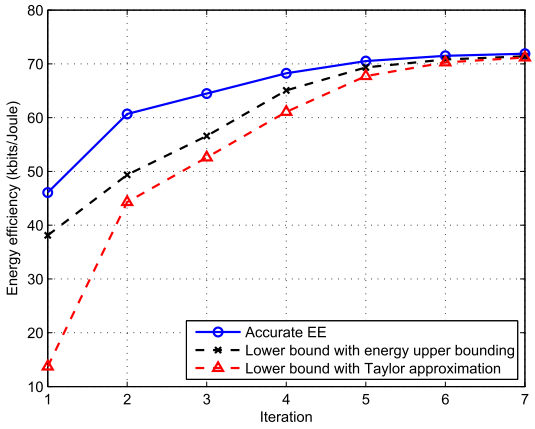

Fig. 4. Convergence of Algorithm 1.

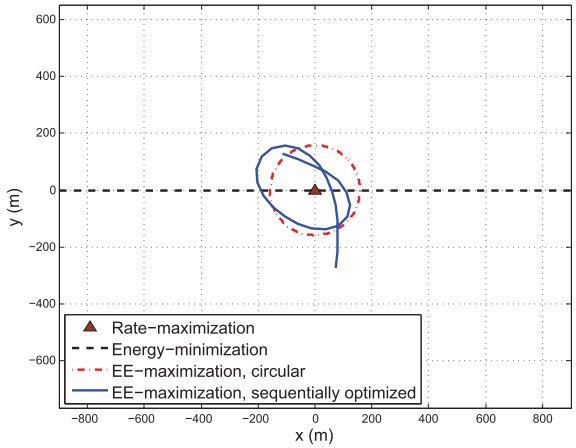

Fig. 5. Trajectory comparison for unconstrained optimization.

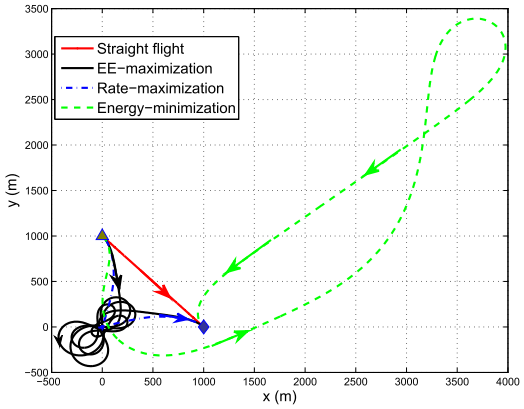

Fig. 6. Trajectory comparison with constrained optimization. The triangle and diamond denote the initial and final UAV locations, respectively.

The communication bandwidth is $B = 1$MHz and the noise power spectrum density at the GT receiver is assumed to be $N_0 = -170$dBm/Hz. Thus, the corresponding noise power is $\sigma^2 = N_0 B = -110$dBm. We assume that the UAV transmission power is $P = 10$dBm (or 0.01W), and the reference channel power is $\beta_0 = -50$dB. As a result, the maximum SNR achieved when the UAV is just above the GT can be obtained as 30dB. Furthermore, we assume that $c_1 = 9.26 \times 10^{-4}$ and $c_2 = 2250$, such that the UAV's energy-minimum speed is $V_{\text{em}} = 30$m/s and the corresponding minimum propulsion power consumption is $P_{\text{em}} = 100$W. Note that we have $P \ll P_{\text{em}}$, thus the UAV transmission power can be practically ignored.

A. Unconstrained Trajectory Optimization

We first consider the case of unconstrained trajectory optimization in the absence of C_1–C_6. Besides the three specific trajectory designs considered in Section III and Section IV, namely the rate-maximization, energy-minimization, and energy-efficient circular designs, the energy-efficiency maximization design by applying the similar sequential convex optimization proposed in Algorithm 1 but without trajectory constraints is also included for comparison.

Under this setup, Fig. 4 shows the convergence of Algorithm 1 with randomly generated initial points, where the terminating threshold of Algorithm 1 is set as $\epsilon = 0.1\%$. Note that Fig. 4 consists of three curves: the "Accurate EE" corresponds to the exact energy efficiency based on the energy consumption model (5), the "Lower bound with energy upper bounding" is that due to the energy upper bounding given in (30), and the "Lower bound with Taylor approximation" corresponds to the optimal value of (P2.2) by using local convex approximation. Fig. 4 shows that Algorithm 1 monotonically converges, as expected from Lemma 1. Furthermore, it also shows that the adopted lower bounds for the purpose of efficient convex optimization are rather tight, especially as the algorithm converges.

Fig. 5 shows the obtained UAV trajectories projected onto the horizontal plane for four different designs with $T = 60$s. As shown in Section III, the unconstrained rate-maximization and energy-minimization trajectories correspond to stationary hovering with $V = 0$ and steady straight flight with power-minimum speed $V_{\text{em}} = 30$m/s, respectively. On the other hand, for the EE-maximization circular trajectory, the optimal flight radius and speed are $r^\star = 158$m and $V^\star = 25.67$m/s, respectively. It is also observed that the obtained trajectory via applying the sequential convex optimization for EE maximization is rather similar to the circular trajectory. Table I gives a detailed comparison for these four different designs in terms of the time-averaged UAV speed, acceleration, achievable communication rate, power consumption, and the overall energy efficiency. It is found that for the unconstrained trajectory setup, the simple circular trajectory with optimized flight radius and speed gives a similar performance as that obtained via sequential convex optimization. This is expected since with both trajectories, the UAV hovers around the GT with smooth turning angles, which achieves a good balance between rate maximization and energy minimization.

B. Constrained Trajectory Optimization

Next, we consider the constrained trajectory optimization as studied in Section V. As shown in Fig. 6, we let $\mathbf{q}_0 = [0,\ 1000]^T$, $\mathbf{q}_F = [1000,\ 0]^T$, $\mathbf{v}_0 = \mathbf{v}_F = 30\vec{\mathbf{v}}_{0F}$, with $\vec{\mathbf{v}}_{0F} \triangleq (\mathbf{q}_F - \mathbf{q}_0)/\|\mathbf{q}_F - \mathbf{q}_0\|$ denoting the direction from $\mathbf{q}_0$ to $\mathbf{q}_F$. Furthermore, the maximum and minimum UAV speed are set

TABLE I
PERFORMANCE COMPARISON FOR VARIOUS DESIGNS WITH UNCONSTRAINED TRAJECTORY OPTIMIZATION

	Average speed (m/s)	Average acceleration (m^2/s)	Average rate (Mbps)	Average power (Watts)	Energy efficiency (kbits/Joule)
Rate-maximization	0	0	9.97	∞	0
Energy-minimization	30	0	6.06	100	60.6
EE-maximization, circular	25.20	4.02	8.16	119.10	68.56
EE-maximization, sequentially optimized	25.67	3.24	8.34	116.02	71.89

TABLE II
PERFORMANCE COMPARISON FOR VARIOUS DESIGNS WITH CONSTRAINED TRAJECTORY OPTIMIZATION

	Average speed (m/s)	Average acceleration (m^2/s)	Average rate (Mbps)	Average power (Watts)	Energy efficiency (kbits/Joule)
Straight flight	3.54	0	4.01	636.44	6.30
Rate-maximization	8.16	4.89	9.53	794.75	11.99
Energy-minimization	29.87	0.73	2.08	101.35	20.52
EE-maximization	25.80	3.05	7.32	116.45	62.86

to $V_{\max} = 100$m/s and $V_{\min} = 3$m/s, respectively, and the maximum acceleration is $a_{\max} = 5\text{m/s}^2$. The operation time is assumed to be $T = 400$s, which is discretized with time step size $\delta_t = 0.2$s. For the sequential convex optimization in Algorithm 1, the initial points are set to be the straight flight from $\mathbf{q}_0$ to $\mathbf{q}_F$ with constant velocity.

Fig. 6 shows the obtained trajectories with the rate-maximization, energy-minimization, and EE-maximization designs, as well as the simple heuristic straight flight from $\mathbf{q}_0$ to $\mathbf{q}_F$ with constant velocity (in this case, the initial and final velocity constraints $\mathbf{v}_0$ and $\mathbf{v}_F$ are ignored). Note that the rate-maximization and energy-minimization trajectories are obtained with the similar sequential convex optimization technique as in Algorithm 1 with the objective function modified accordingly. It is observed from Fig. 6 that besides satisfying the initial and final location constraints, all the three trajectories based on sequential convex optimizations are tangential to the direction vector $\vec{\mathbf{v}}_{0F}$ at both the initial and final locations $\mathbf{q}_0$ and $\mathbf{q}_F$, due to the imposed initial and final velocity constraints. Furthermore, for the rate-maximization trajectory, it is found that the UAV hovers around the GT (i.e., the origin) for the maximum possible duration to maintain the best communication channel. In contrast, the energy-minimization design yields a trajectory mostly following a straight path or with relatively large turning radius since it is in general less power-consuming. However, such a trajectory is expected to incur rather poor communication channels due to the large distance from the GT for most of the time. On the other hand, with the proposed EE-maximization trajectory design, upon approaching the GT, the UAV hovers around following an approximately "8"-shape path, which is expected to maintain a sufficiently good communication channel yet without excessive power consumption.

Fig. 7 plots the time-varying speed of the four trajectories shown in Fig. 6. It is found that for the rate-maximization trajectory, the UAV firstly flies towards the GT with large speed, then gradually reduces its speed to the minimum required value and hovering around the GT, and finally flies towards the destination with increased speed. On the other hand, the energy-minimization and EE-maximization trajectories mostly maintain the speed around the energy-minimum value $V_{\text{em}} = 30$m/s.

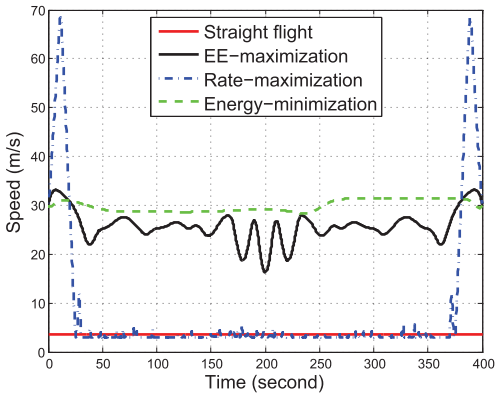

Fig. 7. UAV speed corresponding to the trajectories shown in Fig. 6.

The performance comparison of the above trajectory designs is given in Table II. It is observed that the proposed EE-maximization design achieves a good balance between rate maximization (column 4) and power minimization (column 5), and hence achieves significantly higher energy efficiency (column 6) than the merely rate-maximization and energy-minimization designs. On the other hand, the heuristic straight flight results in the worst energy efficiency, which is expected since it neither maximizes the achievable communication rate nor minimizes the UAV energy consumption.

VII. CONCLUSION

This paper studies the energy-efficient UAV communication via trajectory optimization by taking into account the propulsion energy consumption of the UAV. A theoretical model on the UAV's propulsion energy consumption is derived, based on which the energy efficiency of UAV communication is defined. For the case of unconstrained trajectory optimization,

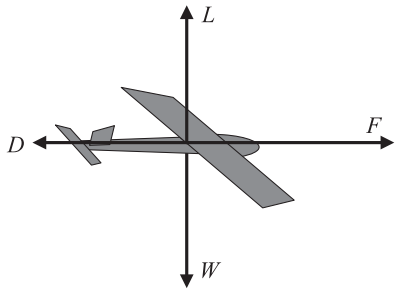

Fig. 8. Schematic of the forces on an aircraft in straight-and-level flight.

it is shown that both the rate-maximization and energy-minimization designs lead to vanishing energy efficiency and thus are energy-inefficient in general. We then consider a practical circular trajectory with optimized flight radius and speed for maximizing energy efficiency. Furthermore, for the generally constrained trajectory optimization, an efficient algorithm is proposed to maximize the energy efficiency based on linear state-space approximation and sequential convex optimization techniques. Numerical results show that the proposed designs achieve significantly higher energy efficiency than that based on rate-maximization or energy-minimization for UAV communications.

Appendix A
Derivation of UAV Propulsion Energy Consumption Model

In this appendix, we derive the propulsion energy consumption model of fixed-wing UAVs with level flight (i.e., flight with a constant altitude). The more general energy consumption model with aircraft ascending and descending will be left as future work.

1) Forces on the Aircraft: As shown in Fig. 8, an aircraft aloft is in general subject to four forces: weight, drag, lift, and thrust [17].

- *Weight* (W): the force of gravity, $W = mg$, with m denoting the aircraft's mass including all its payload, and g is the gravitational acceleration in m/s^2.
- *Drag* (D): the aerodynamic force component parallel to the airflow direction. For zero wind speed, D is in the opposite direction of the aircraft's motion.
- *Lift* (L): the aerodynamic force component normal to the drag and pointing upward.
- *Thrust* (F): the force produced by the aircraft engine, which overcomes the drag to move the aircraft forward.

For an aircraft moving at a subsonic speed V (as usually the case), the drag can be expressed as ([17], eqs. (4.1), (4.2), (4.13), and (4.14))

$$D = \frac{1}{2}\rho C_{D_0} S V^2 + \frac{2L^2}{(\pi e_0 \mathcal{A}_{\mathcal{R}})\rho S V^2}, \tag{55}$$

where ρ is the air density in kg/m^3, C_{D_0} is the zero-lift drag coefficient, S is a reference area (e.g., the wing area), e_0 is the Oswald efficiency (or wing span efficiency) with typical value between 0.7 and 0.85 [17], $\mathcal{A}_{\mathcal{R}}$ is the aspect ratio of the wing, i.e., the ratio of the wing span to its aerodynamic breadth. The first term in (55) is known as the *parasitic drag*, which is a combination of multiple drag components such as form drag, skin friction drag and interference drag, etc. The parasitic drag increases quadratically with the vehicle speed V. The second term in (55) is called the *lift-induced drag*, which is the resulting drag force due to wings redirecting air to generate lift L.

The drag expression (55) can be rewritten as

$$D = c_1 V^2 + \frac{c_2 \kappa^2}{V^2}, \tag{56}$$

where

$$c_1 \triangleq \frac{1}{2}\rho C_{D_0} S, \quad c_2 \triangleq \frac{2W^2}{(\pi e_0 \mathcal{A}_{\mathcal{R}})\rho S} \tag{57}$$

are two constant parameters, and $\kappa \triangleq L/W$ is known as the *load factor*, i.e., the ratio of the aircraft's lift to its weight. Note that to maintain a level flight (i.e., a flight with constant altitude), we must have $\kappa \geq 1$ since the lift must at least balance the aircraft weight to avoid descending. It is then not difficult to conclude from (56) that $\forall V > 0$, we have $D \geq D_{\min}$, where $D_{\min} = 2\sqrt{c_1 c_2}$ is the minimum drag incurred, which corresponds to $\kappa = 1$ and the drag-minimum speed $V_{\rm dm} = (c_2/c_1)^{1/4}$.

2) Power Required for Straight-and-Level Flight: Straight-and-level flight refers to the flight in which a constant heading (or direction) and altitude are maintained. This implies that: (i) the horizontal acceleration, if any, must be in parallel with the aircraft's flying direction so that no turning occurs; (ii) the lift and weight are balanced so that there is no vertical acceleration. We thus have the following equations (as illustrated in Fig. 8):

$$L = W, \quad F - D = ma, \tag{58}$$

where a is the acceleration along the aircraft's flying direction, i.e., $a > 0$ for accelerating and $a < 0$ for decelerating. When $a \geq -D/m$, we have $F \geq 0$. In this case, the thrust F generated by the engine is in the same direction as the aircraft's motion, or *forward thrust*. In contrast, if $a < -D/m$, we have $F < 0$, in which case the thrust F generated by the engine must be in the opposite direction as the aircraft's motion, or *reverse thrust*. One sufficient (but not necessary) condition to ensure forward thrust operation is $a \geq -D_{\min}/m$.

By considering an infinitesimal time interval such that the speed can be regarded as unchanged, it follows from (56) and (58) that the power required for straight-and-level flight with speed V and acceleration a can be expressed as

$$P_{\rm R}(V, a) = |F|V = \left| c_1 V^3 + \frac{c_2}{V} + maV \right|, \tag{59}$$

where we have used the fact that power is equal to force times speed. Note that the magnitude operator in (59) is necessary for the unusual case of reverse thrust with $F < 0$ when the aircraft needs to have an abrupt deceleration.

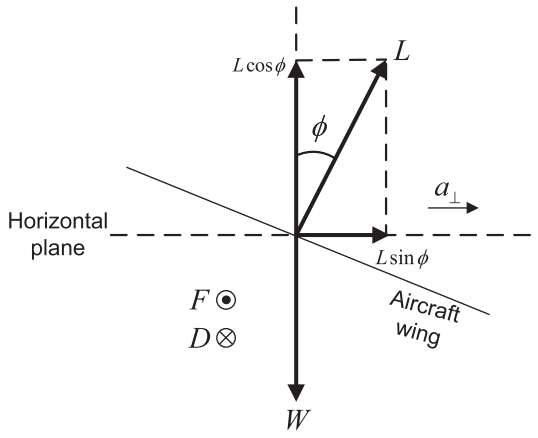

Fig. 9. Schematic of the forces on an aircraft in banked level turn. The aircraft moves normal to the page. The horizontal component of the lift $L\sin\phi$ causes the centrifugal acceleration $a_\perp$ to change the heading.

3) Power Required for Banked Level Turn: For a fixed-wing aircraft to change its flying direction, the aircraft must roll to a banked position so that the lift L generates a lateral (horizontal) component to support the centrifugal acceleration, i.e., the acceleration component normal to the velocity. As illustrated in Fig. 9, let ϕ denote the bank angle, i.e., the angle between the vertical plane and the aircraft's symmetry plane. We then have the following equations,

$$L\cos\phi = W, \quad L\sin\phi = ma_\perp, \tag{60}$$

$$F - D = ma_\parallel, \tag{61}$$

where $a_\perp$ and $a_\parallel$ denote the acceleration components that are perpendicular and parallel to velocity, respectively, with $a_\parallel > 0$ for accelerating and $a_\parallel < 0$ for decelerating. By dividing the two equations in (60), we have

$$\tan\phi = \frac{a_\perp}{g}. \tag{62}$$

In other words, the bank angle ϕ has a one-to-one correspondence with the UAV's centrifugal acceleration $a_\perp$. For instance, for $a_\perp = 5\text{m/s}^2$, we have $\phi = 27°$. As a result, for practical UAVs with a maximum bank angle $\phi_{\max}$ (or correspondingly maximum turning angle), the corresponding maximum centrifugal acceleration can be obtained as $a_\perp^{\max} = g\tan\phi_{\max}$. Besides, it can be obtained from (60) that the load factor for banked level turn is related to the centrifugal acceleration as $\kappa = \sqrt{1 + a_\perp^2/g^2}$. Thus, for banked level turn with $a_\perp \neq 0$, we always have $\kappa > 1$. It then follows from (56) that for the same UAV speed V, banked level turn always incurs a higher drag as compred to straight flight in which case $\kappa = 1$, as expected. Furthermore, with (56) and (61), we have

$$F = c_1 V^2 + \frac{c_2}{V^2}\left(1 + \frac{a_\perp^2}{g^2}\right) + ma_\parallel. \tag{63}$$

Therefore, the instantaneous power required for the banked level turn flight with speed V, tangential acceleration $a_\parallel$, and centrifugal acceleration $a_\perp$ can be expressed as

$$P_{\mathrm{R}}(V, a_\parallel, a_\perp) = |F|V = \left| c_1 V^3 + \frac{c_2}{V}\left(1 + \frac{a_\perp^2}{g^2}\right) + ma_\parallel V \right|. \tag{64}$$

It is not difficult to verify that (59) is a special case of (64) with $a_\perp = 0$.

4) Energy Required for Trajectory $\mathbf{q}(t)$*:* For any given velocity vector $\mathbf{v}$ and acceleration vector $\mathbf{a}$, the tangential and centrifugal accelerations can be obtained by decomposing $\mathbf{a}$ along the parallel and normal directions of $\mathbf{v}$, which gives

$$a_\parallel = \frac{\mathbf{a}^T\mathbf{v}}{\|\mathbf{v}\|}, \quad a_\perp = \sqrt{\|\mathbf{a}\|^2 - \frac{(\mathbf{a}^T\mathbf{v})^2}{\|\mathbf{v}\|^2}}. \tag{65}$$

By substituting (65) and $V = \|\mathbf{v}\|$ into (64), the instantaneous power required as a function of $\mathbf{v}$ and $\mathbf{a}$ can be expressed as

$$P_{\mathrm{R}}(\mathbf{v}, \mathbf{a}) = \left| c_1\|\mathbf{v}\|^3 + \frac{c_2}{\|\mathbf{v}\|}\left(1 + \frac{\|\mathbf{a}\|^2 - \frac{(\mathbf{a}^T\mathbf{v})^2}{\|\mathbf{v}\|^2}}{g^2}\right) + m\mathbf{a}^T\mathbf{v} \right|. \tag{66}$$

For an aircraft with trajectory $\mathbf{q}(t)$, and hence velocity $\mathbf{v}(t) = \dot{\mathbf{q}}(t)$ and acceleration $\mathbf{a}(t) = \ddot{\mathbf{q}}(t)$, the total propulsion energy required is then given by

$$\bar{E}(\mathbf{q}(t)) = \int_0^T P_{\mathrm{R}}\left(\mathbf{v}(t),\ \mathbf{a}(t)\right) dt, \tag{67}$$

with $P_{\mathrm{R}}(\cdot)$ given by (66).

For normal aircraft flight without drastic deceleration so that thrust reversal is not required, the term inside the magnitude operator of (66) is always non-negative. As a result, (67) can be rewritten as

$$\begin{aligned}\bar{E}(\mathbf{q}(t)) &= \int_0^T \left[c_1\|\mathbf{v}(t)\|^3 + \frac{c_2}{\|\mathbf{v}(t)\|}\left(1 + \frac{\|\mathbf{a}(t)\|^2 - \frac{(\mathbf{a}^T(t)\mathbf{v}(t))^2}{\|\mathbf{v}(t)\|^2}}{g^2}\right)\right] dt \\ &\quad + \int_0^T m\mathbf{a}^T(t)\mathbf{v}(t)dt. \end{aligned} \tag{68}$$

Furthermore, the last term in (68) can be expressed as

$$\int_0^T m\mathbf{a}^T(t)\mathbf{v}(t)dt = \int_0^T m\dot{\mathbf{v}}^T(t)\mathbf{v}(t)dt \tag{69}$$

$$= \frac{1}{2}m\left[\|\mathbf{v}(T)\|^2 - \|\mathbf{v}(0)\|^2\right], \tag{70}$$

where the equality in (70) follows from the integral identity $\int \dot{\mathbf{v}}^T(t)\mathbf{v}(t)dt = \frac{1}{2}\|\mathbf{v}(t)\|^2$. This thus completes the derivation of the UAV energy consumption model in (5).

Appendix B
Proof of Theorem 1

To obtain the optimal solution to problem (10), we first consider its relaxed problem by ignoring the equality constraints $\mathbf{a}(t) = \dot{\mathbf{v}}(t)$, $\forall t$, whose optimal value obviously gives a lower bound to that of problem (10). We then show that the optimal solution to this relaxed problem automatically satisfies the equality constraints of problem (10), and thus it is also optimal to (10).

For the relaxed problem, it is evident that the optimal solution should satisfy $\mathbf{a}^\star(t) = \mathbf{0}$. Furthermore, by decomposing the velocity vector $\mathbf{v}(t)$ as $\mathbf{v}(t) = V(t)\vec{\mathbf{v}}(t)$, with $V(t) \geq 0$

and $\|\vec{\mathbf{v}}(t)\| = 1$ denoting the time-varying speed and direction, respectively, the problem reduces to

$$\min_{V(t)} \int_0^T \left[c_1 V^3(t) + \frac{c_2}{V(t)} \right] dt$$
$$\text{s.t. } V(t) \geq 0, \quad \forall t. \tag{71}$$

Lemma 2: The optimum solution to problem (71) *is*

$$V^\star(t) = V_{\text{em}} = \left(\frac{c_2}{3c_1} \right)^{1/4}, \quad \forall t. \tag{72}$$

Proof: First, we show that constant speed is optimal to problem (71). To this end, define the function $f(V) = c_1 V^3 + c_2/V$, which can be shown to be a convex function for $V \geq 0$. For any time-varying speed $V(t)$ over a duration T, let $\bar{V} = \frac{1}{T}\int_0^T V(t)dt$ be the average speed. By applying the Jensen's inequality to the convex function $f(V)$, we have $f(\bar{V}) \leq \frac{1}{T}\int_0^T f(V(t))dt$. Thus, the average speed $\bar{V}$ always achieves a smaller objective value to problem (71). Thus, constant speed is optimal to (71), i.e., $V(t) = V, \forall t$. By setting the first-order derivative of $f(V)$ to zero, the optimal speed in (72) can be obtained. ∎

As a result, the optimal solution to the relaxed problem of (10) is $\mathbf{a}^\star(t) = \mathbf{0}$, $\mathbf{v}^\star(t) = (\frac{c_2}{3c_1})^{1/4}\vec{\mathbf{v}}(t)$, $\forall t$, with $\vec{\mathbf{v}}(t)$ being the arbitrary flying direction. Without loss of optimality, we may set $\vec{\mathbf{v}}(t) = \vec{\mathbf{v}}$, $\forall t$, i.e., by imposing a time-invariant direction. As such, the equality constraint of problem (10) is automatically satisfied since $\mathbf{a}^\star(t) = \dot{\mathbf{v}}^\star(t) = \mathbf{0}$. This thus leads to the optimal solution in (11). The optimal value in (12) can then be obtained accordingly. This completes the proof of Theorem 1.

REFERENCES

[1] Y. Zeng, R. Zhang, and T. J. Lim, "Wireless communications with unmanned aerial vehicles: Opportunities and challenges," *IEEE Commun. Mag.*, vol. 54, no. 5, pp. 36–42, May 2016.

[2] A. Al-Hourani, S. Kandeepan, and S. Lardner, "Optimal LAP altitude for maximum coverage," *IEEE Wireless Commun. Lett.*, vol. 3, no. 6, pp. 569–572, Dec. 2014.

[3] R. I. Bor-Yaliniz, A. El-Keyi, and H. Yanikomeroglu, "Efficient 3-D placement of an aerial base station in next generation cellular networks," in *Proc. IEEE Int. Conf. Commun. (ICC)*, Kuala Lumpur, Malaysia, May 2016, pp. 1–6.

[4] M. Mozaffari, W. Saad, M. Bennis, and M. Debbah, "Efficient deployment of multiple unmanned aerial vehicles for optimal wireless coverage," *IEEE Commun. Lett.*, vol. 20, no. 8, pp. 1647–1650, Aug. 2016.

[5] J. Lyu, Y. Zeng, R. Zhang, and T. J. Lim, "Placement optimization of UAV-mounted mobile base stations," *IEEE Commun. Lett.*, vol. 21, no. 3, pp. 604–607, Mar. 2017.

[6] A. Merwaday and I. Guvenc, "UAV assisted heterogeneous networks for public safety communications," in *Proc. IEEE Wireless Commun. Netw. Conf. (WCNC)*, Mar. 2015, pp. 329–334.

[7] M. Kobayashi, "Experience of infrastructure damage caused by the Great East Japan Earthquake and countermeasures against future disasters," *IEEE Commun. Mag.*, vol. 52, no. 3, pp. 23–29, Mar. 2014.

[8] S. Rohde, M. Putzke, and C. Wietfeld, "Ad hoc self-healing of OFDMA networks using UAV-based relays," *Ad Hoc Netw.*, vol. 11, no. 7, pp. 1893–1906, Sep. 2013.

[9] A. Osseiran *et al.*, "Scenarios for 5G mobile and wireless communications: The vision of the METIS project," *IEEE Commun. Mag.*, vol. 52, no. 5, pp. 26–35, May 2014.

[10] W. Zhao, M. Ammar, and E. Zegura, "A message ferrying approach for data delivery in sparse mobile ad hoc networks," in *Proc. ACM Mobihoc*, May 2004, pp. 187–198.

[11] P. Zhan, K. Yu, and A. L. Swindlehurst, "Wireless relay communications with unmanned aerial vehicles: Performance and optimization," *IEEE Trans. Aerosp. Electron. Syst.*, vol. 47, no. 3, pp. 2068–2085, Jul. 2011.

[12] Y. Zeng, R. Zhang, and T. J. Lim, "Throughput maximization for UAV-enabled mobile relaying systems," *IEEE Trans. Commun.*, vol. 64, no. 12, pp. 4983–4996, Dec. 2016.

[13] B. Pearre and T. X. Brown, "Model-free trajectory optimization for wireless data ferries among multiple sources," in *Proc. IEEE Global. Commun. Conf. (GLOBECOM)*, Miami, FL, USA, Dec. 2010, pp. 1793–1798.

[14] J. Lyu, Y. Zeng, and R. Zhang, "Cyclical multiple access in UAV-aided communications: A throughput-delay tradeoff," *IEEE Wireless Commun. Lett.*, vol. 5, no. 6, pp. 600–603, Dec. 2016.

[15] Y. Chen *et al.*, "Fundamental trade-offs on green wireless networks," *IEEE Commun. Mag.*, vol. 49, no. 6, pp. 30–37, Jun. 2011.

[16] Z. Hasan, H. Boostanimehr, and V. K. Bhargava, "Green cellular networks: A survey, some research issues and challenges," *IEEE Commun. Surveys Tuts.*, vol. 13, no. 4, pp. 524–540, Nov. 2011.

[17] A. Filippone, *Flight Performance of Fixed and Rotary Wing Aircraft*. Washington, DC, USA: AIAA, 2006.

[18] E. I. Grotli and T. A. Johansen, "Path planning for UAVs under communication constraints using SPLAT! and MILP," *J. Intell. Robot. Syst.*, vol. 65, no. 1, pp. 265–282, 2012.

[19] C. D. Franco and G. Buttazzo, "Energy-aware coverage path planning of UAVs," in *Proc. IEEE Int. Conf. Auto. Robot Syst. Compet.*, Apr. 2015, pp. 111–117.

[20] S. Kandeepan, K. Gomez, L. Reynaud, and T. Rasheed, "Aerial-terrestrial communications: Terrestrial cooperation and energy-efficient transmissions to aerial base stations," *IEEE Trans. Aerosp. Electron. Syst.*, vol. 50, no. 4, pp. 2715–2735, Oct. 2014.

[21] M. Mozaffari, W. Saad, M. Bennis, and M. Debbah, "Optimal transport theory for power-efficient deployment of unmanned aerial vehicles," in *Proc. IEEE Int. Conf. Commun. (ICC)*, Kuala Lumpur, Malaysia, May 2016, pp. 1–6.

[22] K. Li, W. Ni, X. Wang, R. P. Liu, S. S. Kanhere, and S. Jha, "Energy-efficient cooperative relaying for unmanned aerial vehicles," *IEEE Trans. Mobile Comput.*, vol. 15, no. 6, pp. 1377–1386, Jun. 2016.

[23] F. Jiang and A. L. Swindlehurst, "Optimization of UAV heading for the ground-to-air uplink," *IEEE J. Sel. Areas Commun.*, vol. 30, no. 5, pp. 993–1005, Jun. 2012.

[24] K. Anazawa, P. Li, T. Miyazaki, and S. Guo, "Trajectory and data planning for mobile relay to enable efficient Internet access after disasters," in *Proc. IEEE Global. Commun. Conf. (GLOBECOM)*, San Diego, LA, USA, Dec. 2015, pp. 1–6.

[25] Z. Han, A. L. Swindlehurst, and K. J. R. Liu, "Optimization of MANET connectivity via smart deployment/movement of unmanned air vehicles," *IEEE Trans. Veh. Technol.*, vol. 58, no. 7, pp. 3533–3546, Sep. 2009.

[26] S. Kim, H. Oh, J. Suk, and A. Tsourdos, "Coordinated trajectory planning for efficient communication relay using multiple UAVs," *Control Eng. Pract.*, vol. 29, pp. 42–49, May 2014.

[27] T. Schouwenaars, B. D. Moor, E. Feron, and J. How, "Mixed integer programming for multi-vehicle path planning," in *Proc. Eur. Control Conf.*, Sep. 2001, pp. 2603–2608.

[28] A. Richards and J. P. How, "Aircraft trajectory planning with collision avoidance using mixed integer linear programming," in *Proc. Amer. Control Conf.*, May 2002, pp. 1936–1941.

[29] A. Goldsmith, *Wireless Communications*. Cambridge, U.K.: Cambridge Univ. Press, 2005.

[30] C. Desset *et al.*, "Flexible power modeling of LTE base stations," in *Proc. IEEE Wireless Commun. Netw. Conf. (WCNC)*, Apr. 2012, pp. 2858–2862.

[31] E. M. Greitzer, Z. S. Spakovszky, and I. A. Waitz. *Thermodynamics & Propulsion, 16. Unified, MIT Course Notes*. Accessed on Jul. 5, 2016. [Online]. Available: http://web.mit.edu/16.unified/www/FALL/thermodynamics/notes/notes.html

[32] H. D. Young, *University Physics With Modern Physics*, 13th ed. Reading, MA, USA: Addison-Wesley, 2011.

[33] S. Boyd and L. Vandenberghe, *Convex Optimization*. Cambridge, U.K.: Cambridge Univ. Press, 2004.

[34] J.-P. Crouzeix and J. A. Ferland, "Algorithms for generalized fractional programming," *Math. Programm.*, vol. 52, no. 1, pp. 191–207, 1991.

[35] A. Zappone, E. Björnson, L. Sanguinetti, and E. Jorswieck. (2016). "Achieving global optimality for energy efficiency maximization in wireless networks." [Online]. Available: https://arxiv.org/abs/1602.02923

Yong Zeng (S'12–M'14) received the B.Eng. degree (Hons.) in electrical and electronic engineering and the Ph.D. degree in electrical and electronic engineering from Nanyang Technological University, Singapore, in 2009 and 2014, respectively. In 2010, he was an intern student with the Research and Innovation Center (Bell Labs China), Alcatel-Lucent Shanghai Bell Company, Ltd., China. Since 2013, he has been a Research Fellow with the Department of Electrical and Computer Engineering, National University of Singapore. His current research interests include MIMO transceiver optimization for wireless systems, wireless power transfer, massive MIMO, millimeter wave communications, UAV communications, and other 5G related topics.

Rui Zhang (S'00–M'07–SM'15–F'17) received the B.Eng. degree (Hons.) and the M.Eng. degree from the National University of Singapore, Singapore, in 2000 and 2001, respectively, and the Ph.D. degree from the Stanford University, Stanford, CA, USA, in 2007, all in electrical engineering.

From 2007 to 2010, he was with the Institute for Infocomm Research, A*STAR, Singapore, where he currently holds a Senior Scientist joint appointment. In 2010, he joined the Department of Electrical and Computer Engineering, National University of Singapore, where he is an Associate Professor and the Dean's Chair with the Faculty of Engineering. He has authored over 250 papers. He has been listed as a Highly Cited Researcher (also known as the World's Most Influential Scientific Minds), by Thomson Reuters, since 2015. His research interests include energy-efficient and energy-harvesting-enabled wireless communications, wireless information and power transfer, multiuser MIMO, cognitive radio, UAV communications, wireless information surveillance, and optimization methods.

Dr. Zhang was the recipient of the Sixth IEEE Communications Society Asia-Pacific Region Best Young Researcher Award in 2011 and the Young Researcher Award of National University of Singapore in 2015. He was a co-recipient of the Best Paper Award from the IEEE PIMRC in 2005, the IEEE Marconi Prize Paper Award in Wireless Communications in 2015, the IEEE Communications Society Asia-Pacific Region Outstanding Paper Award in 2016, and the IEEE Signal Processing Society Best Paper Award in 2016. He has served for over 30 international conferences as a TPC co-chair or an organizing committee member, and as the guest editor of eight special issues in IEEE and other internationally refereed journals. He has been an elected member of the IEEE Signal Processing Society SPCOM and SAM Technical Committees, and served as the Vice-Chair of the IEEE Communications Society Asia-Pacific Board Technical Affairs Committee. He has served as an Editor of the IEEE TRANSACTIONS ON WIRELESS COMMUNICATIONS and the IEEE JOURNAL ON SELECTED AREAS IN COMMUNICATIONS (Green Communications and Networking Series). He is an Editor of the IEEE TRANSACTIONS ON SIGNAL PROCESSING and the IEEE TRANSACTIONS ON GREEN COMMUNICATIONS AND NETWORKING.